Constricted Migration and Differentiation of Human Myoblasts

By

CASSIDY J. MILETI

THESIS

Submitted in partial satisfaction of the requirements for the degree of

MASTER OF SCIENCE

in

BIOMEDICAL ENGINEERING

in the

OFFICE OF GRADUATE STUDIES

of the

UNIVERSITY OF CALIFORNIA

DAVIS

Approved:

Lucas Smith, Chair

J. Kent Leach

Daniel Starr

Committee in Charge

2022

Acknowledgements

I would like to express my deepest gratitude to my advisor, Dr. Lucas Smith, for his mentorship, his confidence in my strengths as a scientist, and his dedication to my learning. I could not have succeeded without his encouragement to explore my interests, both personal and professional, and his constant support as I reevaluated my goals and changed course on my academic journey.

I am also grateful to Dr. Alastair Khodabukus for taking the time to speak with me about his work with tissue-engineered skeletal muscle and offering advice as I began adapting his design. I would also like to acknowledge my committee members, Dr. Kent Leach, from whom I learned much about tissue engineering and working with hydrogels, and Dr. Daniel Starr, who offered new perspectives on nuclear mechanics.

I would also like to recognize my peers in the MyoMatrix Lab, who provided friendship and were always willing to lend a hand with my research and help me solve problems. Lastly, I am thankful for my loved ones, who believed in me and cheered me on every step of the way, and kept me from feeling isolated even at the height of a pandemic. I am so fortunate to have been surrounded by people who supported me and celebrated my achievements.

———

This material is based upon work supported by the NSF Graduate Research Fellowship No. 2036201. Any opinion, findings, and conclusions or recommendations expressed in this material are those of the author and do not necessarily reflect the views of the National Science Foundation.

Abstract

Muscle regeneration depends on satellite cells which, prior to injury, are quiescent and located on the periphery of myofibers. When an injury occurs, satellite cells are activated and migrate to the injury to fuse with damaged myofibers and rebuild the tissue. In certain muscle diseases, such as Duchenne muscular dystrophy (DMD), satellite cells do not function properly and do not effectively regenerate tissue. DMD is characterized by chronic fibrosis, where an excess of collagen builds up and replaces functional tissue. We propose that satellite cells undergo damage when migrating through small spaces in the dense fibrotic tissue. In this thesis, we demonstrate that human myoblasts, active cells already committed to a myogenic lineage, undergo high levels of nuclear rupture and incur DNA damage when migrating through small-diameter pores. They also exhibit impaired adhesion and differentiation, indicating that constricted migration can impair the regenerative capacity of cells.

Tissue engineering can be used to improve studies of muscle cells. We present a platform to grow muscle microtissues from human myoblasts using an extracellular matrix (ECM) protein-based hydrogel for structural and signaling support. This platform has the potential to expand and improve *in vitro* studies of muscle, including studies aimed at understanding the interactions between the muscle ECM and muscle resident cells. It can be customized to model fibrotic diseases using collagen, and it can be used as an additional measure of myoblast function following constricted migration with increased physiological relevance.

Chapter 1. Background

Stem cells are essential to fetal development, but they also play important roles in many adult functions. In skeletal muscle, muscle stem cells, also called satellite cells, enable efficient regeneration after injury [1–4]. In healthy muscle, satellite cells are quiescent and sit on the periphery of muscle fibers, just below the basal lamina [4,5]. When a muscle fiber is injured, the satellite cells are activated by biochemical signals originating at the site of the injury. When activated, satellite cells proliferate and migrate to the site of injury, differentiating and fusing with the damaged myofibers to repair them and provide new myonuclei.

Typically, satellite cells are very effective at repairing muscle, but they can lose their regenerative capacity due to aging or disease. Duchenne muscular dystrophy (DMD), a severe, X-linked disease that occurs in 15.9 to 19.5 per 100,000 live births, is a notable example of one such disease, characterized by muscle fragility and weakness that worsens with age [6].

DMD has no cure, and patients deteriorate quickly after they reach about 7 years old [7]. They typically require the use of a wheelchair by the age of 12 and develop respiratory insufficiency and cardiomyopathy a few years later [7]. These conditions continue to worsen with time, and eventually, the systems fail, leading to premature death between 20 and 40 years of age [8].

In Duchenne muscular dystrophy, muscle cells lack the dystrophin protein due to a genetic mutation in the *DMD* gene. Dystrophin is a key part of the dystrophin-associated protein complex (DAPC), which translates force from the actin cytoskeleton of the myofiber to the surrounding extracellular matrix (ECM) [9]. The disassembly of the DAPC weakens the sarcolemma and impairs important signaling functions, leaving muscle fibers prone to damage and degeneration [8,9].

Following damage, DMD muscle fibers fail to regenerate effectively, with new fibers

remaining small and prone to branching and degeneration [10–12]. This impaired regeneration is due in part to satellite cell dysfunction, despite the fact that the DAPC is not present in satellite cells [9,13]. Satellite cells isolated from patients with DMD exhibit impaired growth kinetics and increased DNA damage [14,15].

The cause of satellite cell dysfunction in DMD is not certain. Satellite cells isolated from the *mdx* mouse model of muscular dystrophy are able to effectively contribute to regeneration in healthy donor muscle, so it has been suggested that their impaired regenerative capacity may be a result of the pathologic environment, rather than endogenous factors as had been previously suspected [11,12,16].

One key element of the pathologic DMD environment that may contribute to impaired regeneration is its progressive fibrosis. Fibrosis is characterized by excessive accumulation of extracellular matrix (ECM) proteins, particularly collagen-rich scar tissue [17]. During normal muscle regeneration after an acute injury, inflammatory macrophages infiltrate the muscle, clearing damaged tissue, and temporary ECM is produced to stabilize the tissue [11,17]. This excess ECM is degraded after the muscle is repaired with functional tissue. Chronic fibrosis occurs when the balance of this process is off, leading to too much ECM production and too little ECM degradation [18].

Pathologic fibrosis occurs following repeated cycles of muscle injury and repair, so it is prevalent in DMD. Fibrosis predicts poor motor outcomes in DMD, indicating that it plays a significant role in the progression of the disease [19,20]. This effect may be mediated in part by fibrosis causing the DNA damage seen in satellite cells isolated from DMD patients [15,21]. This thesis explores the effect of the fibrotic environment on human muscle progenitor function.

Chapter 2. Constricted Migration of Human Myoblasts

Introduction

Muscle fibers are multinucleated cells ensheathed by a layer of extracellular matrix termed the basal lamina. The myonuclei within these fibers are post-mitotic, so they depend on satellite cells to repair injuries and replace myonuclei. When a muscle injury occurs, whether due to trauma, resistance training, or disease, muscle regeneration is initiated [22]. As necrosis occurs in the damaged myofibers, they induce inflammatory responses that clear the debris and release cytokines that contribute to the activation of satellite cells [22].

Upon activation, satellite cells begin to proliferate, migrate, and differentiate. Proliferation has two key purposes – to ensure that there are sufficient myogenic progenitors to contribute to regeneration, and to maintain the population of quiescent cells in the satellite cell niche [3].

Because quiescent satellite cells reside along the myofiber periphery, they must travel from the satellite cell niche to the site of an injury. Satellite cells have high migratory capacity; they tend to move along a single fiber, but there is evidence that they may also travel between adjacent muscles [23–25]. Though they are initially located beneath the basal lamina, following activation, satellite cells exit the niche and adhere instead to the myofiber exterior [23].

The endomysium, which is the layer of extracellular matrix (ECM) that surrounds and separates individual muscle fibers, is estimated to have a thickness of only 0.2μm – 1μm, meaning that satellite cells migrate through tight interstitial spaces even in healthy muscle [26]. In fibrotic muscle, these interstitial spaces are likely even more constricting given the increased density and stiffness of the matrix due to the excess of ECM proteins [27–29]. In addition, the balance of matrix metalloproteinases (MMPs), which break down the ECM, and tissue inhibitors of metalloproteinases (TIMPs), which inhibit ECM breakdown are also out of balance in a fibrotic

environment [30] This means that satellite cells in fibrotic muscle are less able to remodel their surrounding microenvironment, a necessary function that would allow them to create larger interstitial spaces through which they could migrate more easily.

The migration of cells through tight spaces that cause the nucleus to deform is referred to as constricted migration. This phenomenon has been most thoroughly studied as it relates to cancer metastasis, where it has been found to cause nuclear rupture, DNA damage, and cell-cycle inhibition [31–33]. Nuclear rupture and DNA damage have also been observed following constricted migration of healthy mouse myoblasts as well as following typical migration of mutant mouse myoblasts with impaired nuclear stability [21,34].

Given these observations, we were interested in the effect of constricted migration on human myoblasts to determine if these more relevant cells behaved similarly to mouse myoblasts. We used transwell cell culture inserts with porous membranes to model constricted migration in an immortalized human skeletal muscle myoblast cell line. We found an increase in nuclear rupture and DNA damage following migration through 3μm-diameter pores. Additionally, we determined that constricted migration also causes deficits in adhesion and differentiation. Interestingly, we did not find any effect on apoptosis, meaning that it is likely not a contributing factor to the functional differences. These findings show that human myoblasts incur nuclear damage during migration through 3μm pores, beyond that of mouse myoblasts, and demonstrate impaired functionality following constricted migration.

Methods

Culture of Human Myoblasts

hTERT/cdk4-immortalized human myoblasts (Center for Research in Myology) were cultured in growth medium containing DMEM and Medium 199 at a 4:1 volume ratio, supplemented with

20% fetal bovine serum, 25μg/mL fetuin, 5ng/mL human epidermal growth factor, 0.5 ng/mL basic fibroblast growth factor, 5 μg/mL insulin, 0.2 μg/mL dexamethasone, and 1% penicillin-streptomycin [35]. Cells were cultured in tissue culture-treated flasks and incubated at 37°C and 5% carbon dioxide. Cells were passaged at 70-80% confluency and were used from passage 3 to passage 10.

Transwell Migration

To analyze nuclear rupture and DNA damage, we studied cell migration through permeable Falcon FluoroBlok 24-Well cell culture inserts (Fisher Scientific) with membrane pore diameters of either 3μm or 8μm. Cells were seeded on the inserts at a density of 1.67×10^5 cells/cm^2. Growth medium was added to both the top of the inserts and to the well below, and cells were incubated for 48 hours to allow for migration to the bottom of the transwell membrane. (Fig. 1A). Cells were also cultured in wells without inserts as a control. After 48 hours, cells were fixed on both sides of the membrane for immunostaining using 4% paraformaldehyde (Fig. 1B).

For experiments requiring use of migrated cells for further culture, Olympus transparent 6-well cell culture inserts (Genessee) were used with the same pore sizes. Cells were seeded at a concentration of 1.07×10^5 cells/cm^2. Cells were incubated and allowed to migrate for 48 hours, along with control cells in a well without an insert, labelled the 2D condition. Following migration, 0.25% Trypsin EDTA solution (Fisher) was applied to both the top and bottom of the membrane, and inserts were manually agitated such that all non-migrated cells remained on the top of the insert, and the migrated cells fell off the bottom of the insert into the well below. Cells were then collected, counted, and plated for the next part of the experiment (Fig. 1C).

Post-Migration Assays

Following migration and collection, cells were suspended in growth media and were plated

on 96-well tissue culture plates to assess either differentiation or adhesion.

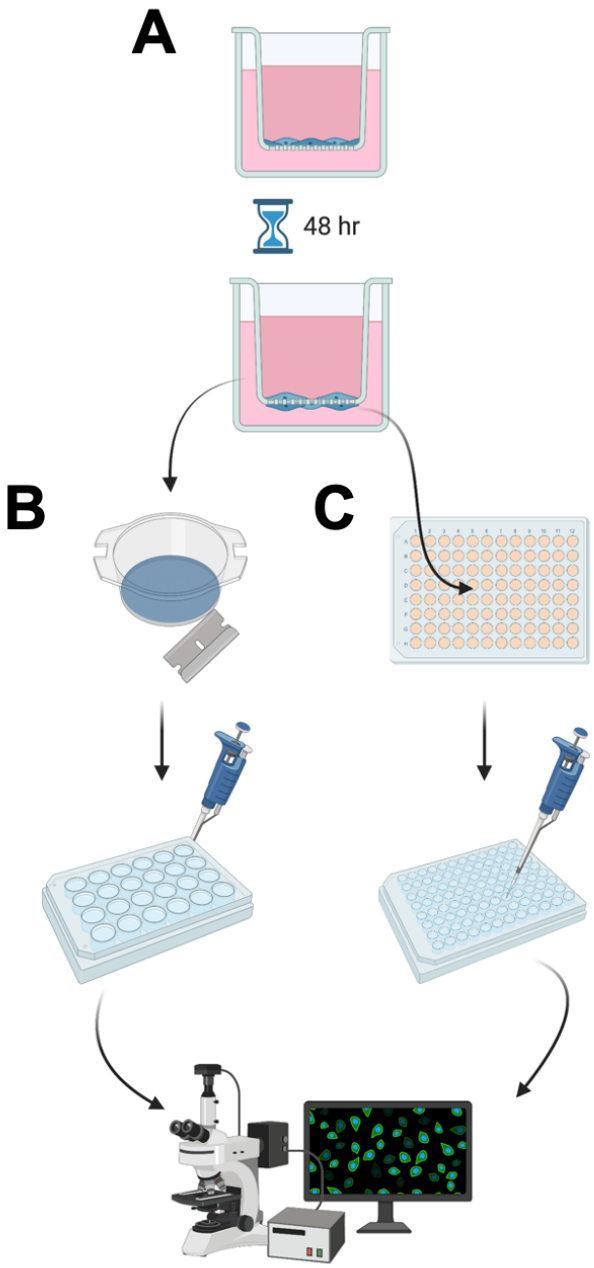

Figure 1: Diagram of transwell assays. (A) Cells are seeded on the top of the transwell inserts and left for 48 hours, during which they migrate through the pores (3µm or 8µm) to the bottom of the transwell. (B) To look at nuclear rupture and DNA damage, the membranes of the inserts are cut and immunostained in a plate prior to imaging. (C) For differentiation and adhesion assays, cells are removed from the bottom of the transwell insert and transferred to a 96-well plate. Following the specified length of time, they are fixed and immunostained prior to imaging. (Created with Biorender.com)

To measure differentiation, cells were seeded at 1.5×10^5 cells/cm^2 on Matrigel-coated plates. Cells were left in growth media overnight to allow them to adhere to the plate and then were switched to differentiation media (DMEM supplemented with 50µg/mL gentamycin and 10µg/mL insulin). Plates were fixed with 4% paraformaldehyde after 3, 5, and 7 days of differentiation. They were stained for myosin heavy chain (MyHC, 1:500) and DNA (Hoechst, 1:1000), then imaged and analyzed in ImageJ to quantify the differentiation index, calculated as the percentage of nuclei that reside in myotubes.

For adhesion, cells were also plated in complete growth media at a concentration of 1.5×10^5 cells/cm^2 on uncoated plates. The plates were incubated at 37°C for either one hour or four hours, then fixed, and DNA and the actin cytoskeleton were

labelled with Hoechst and ActiStain. The same protocol was followed, but with a lower initial cell concentration (3×10^4 cells/cm^2) to assess cell spreading.

Cells were also assayed for apoptosis and necrosis following migration. Immediately after collecting cells from the bottom of inserts and from the control (no migration) well, they were labelled using an apoptosis/necrosis assay kit targeting phosphatidylserine exposure (Abcam, ab176750). 10µL of the cell suspension was transferred to a Countess™ slide to facilitate fluorescent imaging.

Immunostaining

Immunostaining was performed on 96 well plates using standard techniques. Briefly, cells were fixed in 4% paraformaldehyde (Fisher Scientific) for 15 minutes then washed with PBS. Cells were permeabilized with 0.5% Triton-X (Fisher Scientific) for 15 minutes and blocked with 5% BSA for 30 minutes before applying primary antibodies (diluted in 5% BSA). After overnight incubation with primary antibodies at 4°C, plates were washed with 0.1% BSA and secondary antibodies (diluted in 0.1% BSA) were applied for 90 minutes. Conjugated antibodies were applied with the secondary antibodies. The primary antibodies used were skeletal muscle myosin heavy chain (1:500, mouse, MF-20, DHSB), 53BP1 (1:300, rabbit, NB100-904, Novus), phosphorylated histone H2AX (1:500, mouse, 05-636, Millipore), Lamin A/C Alexaflour 488 (1:200, mouse, 8617s, Cell Signaling Technologies), Lamin B (1:500, rabbit, AB16048, ABCAM), Anti-mouse 488 (1:500, donkey, A32766, Invitrogen), Anti-rabbit 555 and 647 (1:500, donkey, A32794 and A32795, Invitrogen), ActiStain 555 (1:250, phalloidin, PHDH7, Cell Signaling Technologies). Finally, DNA was labeled using Hoechst 33342 (Thermo Fisher), applied for 15 minutes then replaced with PBS. To stain FluoroBlok transwell membranes, a similar protocol was followed. Before staining, the membranes were removed from the plastic insert using a razor and placed in

wells. After staining, the membranes were placed on a large coverslip with Prolong Gold. A second coverslip was placed on top and sealed with CoverGrip Coverslip Sealant.

Imaging and Image Analysis

An inverted Leica DMi8 microscope was used to image immunostained cells using epifluorescence. All images within each experiment were taken using the same microscope parameters.

Image analysis was performed using FIJI/ImageJ. All analyses were performed on images with background subtraction applied using an appropriate radius. The images were not otherwise processed for quantification, but the representative images were brightened and sharpened after quantification to make features clearer.

DNA Damage and Nuclear Blebbing

Imaging of cells on FluoroBlock membranes stained for Lamin A/C and Lamin B1 was performed with the 40× objective at randomly selected positions until at least 100 nuclei per membrane were imaged. Cells stained for 53BP1 and γH2AX were imaged using the 63× oil immersion objective. Z-stacks were taken at random positions to ensure all foci in the field were in focus.

Nuclear blebs were quantified manually by counting the number of total cells and the number of cells that demonstrated blebbing (protrusions from the nucleus which contained Lamin A/C but not Lamin 1B), and calculating the percentage of cells that had blebs (Figure 2A).

DNA damage was analyzed using custom ImageJ scripts and MATLAB code. Briefly, the z-stacks were processed using the Stack Focuser plugin by Michael Umorin (kernel = 11) to create a single-plane, focused image [36]. After converting the image to binary, nuclei were manually selected and added to the ROI manager, ensuring that partial nuclei on the edges of the image were

excluded. A threshold was calculated based on the inflection point of the distribution of the number of maxima at every 10 prominence values from 10 to 10,000. This threshold was used as the prominence value to determine the number of maxima representing foci inside each nucleus. γH2AX and 53BP1 were analyzed separately with different threshold values.

Differentiation and Adhesion

Post-migration cells on 96 well plates were imaged with the 20× objective. Differentiation images were taken at 4 random positions per well with three wells for each condition; i.e. 12 images per condition per experiment. Adhesion images were taken as 6x6 merged tile scans centered in the middle of each well, with 4-5 wells per experiment.

Differentiation was quantified using a custom script in FIJI. The nuclei were identified and the intensity of the myosin heavy chain signal surrounding the nuclei was measured. Nuclei were considered to be inside a myotube if the myosin heavy chain signal was above a manually identified threshold, which was kept constant for all replicates within a given experiment but varied between experiments due to differences in imaging parameters. The differentiation index was calculated as the percentage of the total nuclei that were inside myotubes.

Adhesion and cell spreading were also analyzed in FIJI using custom scripts. The nuclei were identified using the Analyze Particles function. The number of nuclei was divided by the area of the merged image to calculate cells per centimeter squared. The actin channel was smoothed 100 times with the built-in smooth function in FIJI to blur cytoskeletal features and enable the user to convert the image to binary to determine the total area the actin covered. This number was divided by the total number of cells to determine the average actin area per cell.

Apoptosis

To assess apoptosis, cells were imaged at 20x in single-cell suspension using a Countess slide.

Because the cells were relatively sparse, images were not taken randomly, but were taken at locations with cells, identified using phase microscopy, until approximately 100 cells were imaged.

Apoptosis and necrosis were also quantified in FIJI. For apoptosis, live nuclei were identified either manually or using the Analyze Particles function in the CytoCalcein Violet channel, and the intensity of the Apopxin signal in the area surrounding the nuclei was measured. Necrotic nuclei were identified manually based on the Nuclear Green DCS1 dye signal, and apoptotic signal surrounding necrotic nuclei was also measured. Because the apoptotic signal was punctate, the maximum intensity in the area was used to identify apoptotic cells. A threshold over which a cell was counted as apoptotic was determined for each experiment based on manual observation. The percentages of apoptotic live cells, apoptotic necrotic cells, and necrotic cells out of the total cells were calculated.

Statistical Analysis

When quantifying DNA damage, the number of foci per cell on the bottom of the transwell was normalized to the average number of foci on the top of each transwell, and the mean was calculated. At least 50 cells were analyzed for each condition, and the experiment was repeated three times. T-tests were performed comparing the means of the three experiments for the top vs. bottom for each condition. Lamin analysis was performed the same way, but the values were not normalized as they were already percentages. Two-way ANOVA was used to determine differences in adhesion, differentiation, and cell spreading with Tukey's multiple comparisons test used for further analysis. One-way ANOVA with Tukey's multiple comparisons test was used for apoptosis.

Results

DNA Damage and Nuclear Blebbing Increase Following Constricted Migration

To determine the effect of constricted migration on human myoblasts, cells were seeded on FluoroBlok inserts and allowed to migrate through pores that were either 3μm or 8μm in diameter for 48 hours (Figure 1). Myoblast nuclei are typically about 10-15μm in diameter, meaning that the nuclei are highly constricted when migrating through the 3μm pores, and minimally constricted through the 8μm pores.

Following migration through 3μm pores, 84% of human myoblasts exhibited nuclear blebs, which are small protrusions containing lamin A/C but depleted of lamin B (Figure 2, A and B). This indicates a high occurrence of nuclear rupture [21,31,32]. In contrast, almost no evidence of blebs was found in cells on the bottoms of the 8μm inserts or in the unmigrated cells that remained on the tops of inserts (Figure 2, A and B). After 48 hours, the 8μm membranes have a similar number of cells on the bottom and the top – around 70,000 cells/cm^2 – while the 3μm membranes have about 85% fewer cells on the bottom of the membrane – 14,000 cells/cm^2 – than the top, with about 90,000 cells/cm^2, emphasizing the difficulty migrating through the small pores. Similarly, the constricted nuclei were deformed and elongated, while the 8μm nuclei maintained a more circular shape akin to the unmigrated cells on top of the membranes (Figure 2A).

The phosphorylation of histone H2AX (γH2AX) marks DNA double strand breaks and plays an important role in initiating the DNA damage response [37]. Therefore, DNA damage following migration was quantified by calculating the ratio of the average foci per cell on the bottom of inserts compared to the top. There were 80% more γH2AX foci per cell on the bottom of 3μm inserts than the top, whereas there was no significant increase in foci in cells that migrated through 8μm pores (Figure 2, C and D).

53BP1, a p53 binding protein, also plays a role in the DNA damage response, further downstream than γH2AX [37,38]. It was used as another measure to quantify DNA damage in the

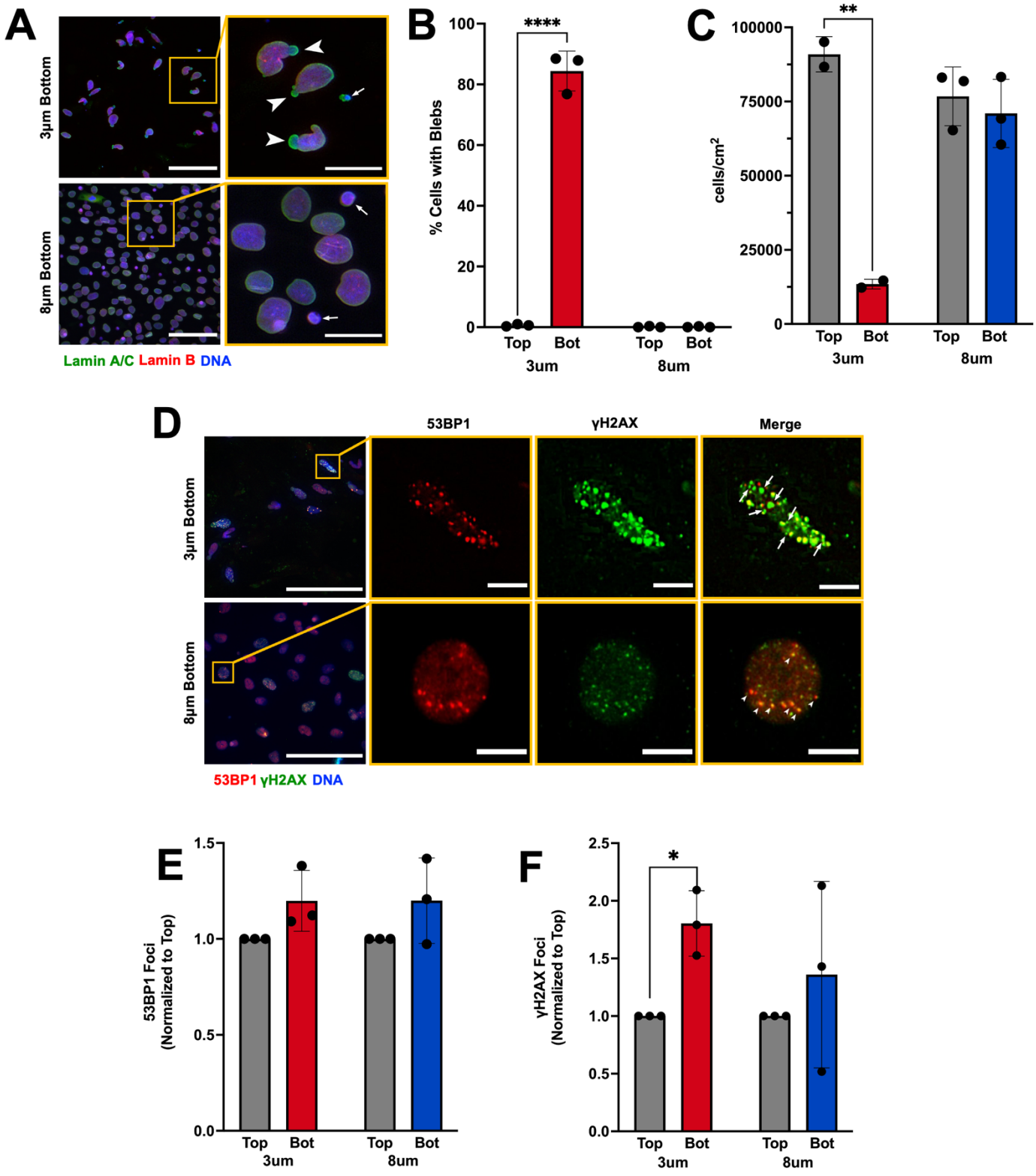

Figure 2: Constricted migration through transwell membranes. (A) Images of nuclei following migration with Lamin A/C, Lamin B, and DNA labeled. Arrowheads point to nuclear blebs. Arrows point to cells that had partially migrated at the time of fixation, demonstrating the approximate size of the pores. Scale bar = 100µm; inset scale bar = 30µm. (B) Quantification of the percentage of cells on the top (no migration) and bottom (post-migration) of the membranes. (C) Images of nuclei following migration with DNA damage markers γH2AX and 53BP1 labeled. Arrows indicate foci that are positive for γH2AX but not 53BP1; Arrowheads indicate foci that are positive for both γH2AX and 53BP1. Scale bar = 100µm; Inset scale bar = 10µm. (D) Quantification of the number of γH2AX foci on bottom of membranes relative to the foci on top of the membranes. (E) Quantification of the number of 53BP1 foci on bottom of membranes relative to the foci on top of the membranes. * = $p < 0.05$, **** = $p < 0.0001$

same manner, but no differences were found in numbers of foci (Figure 2, C and E). There are typically fewer 53BP1 foci than γH2AX foci in a given cell, and each 53BP1 focus is colocalized with a γH2AX focus (Figure 2C) [39].

Constricted Migration Impairs Myoblast Differentiation

Myoblasts readily differentiate and fuse to form multinucleated myotubes. Mouse myoblasts exhibit delayed differentiation following constricted migration, so we hypothesized that we would also see impaired differentiation in human myoblasts [21]. Cells were removed from the bottom

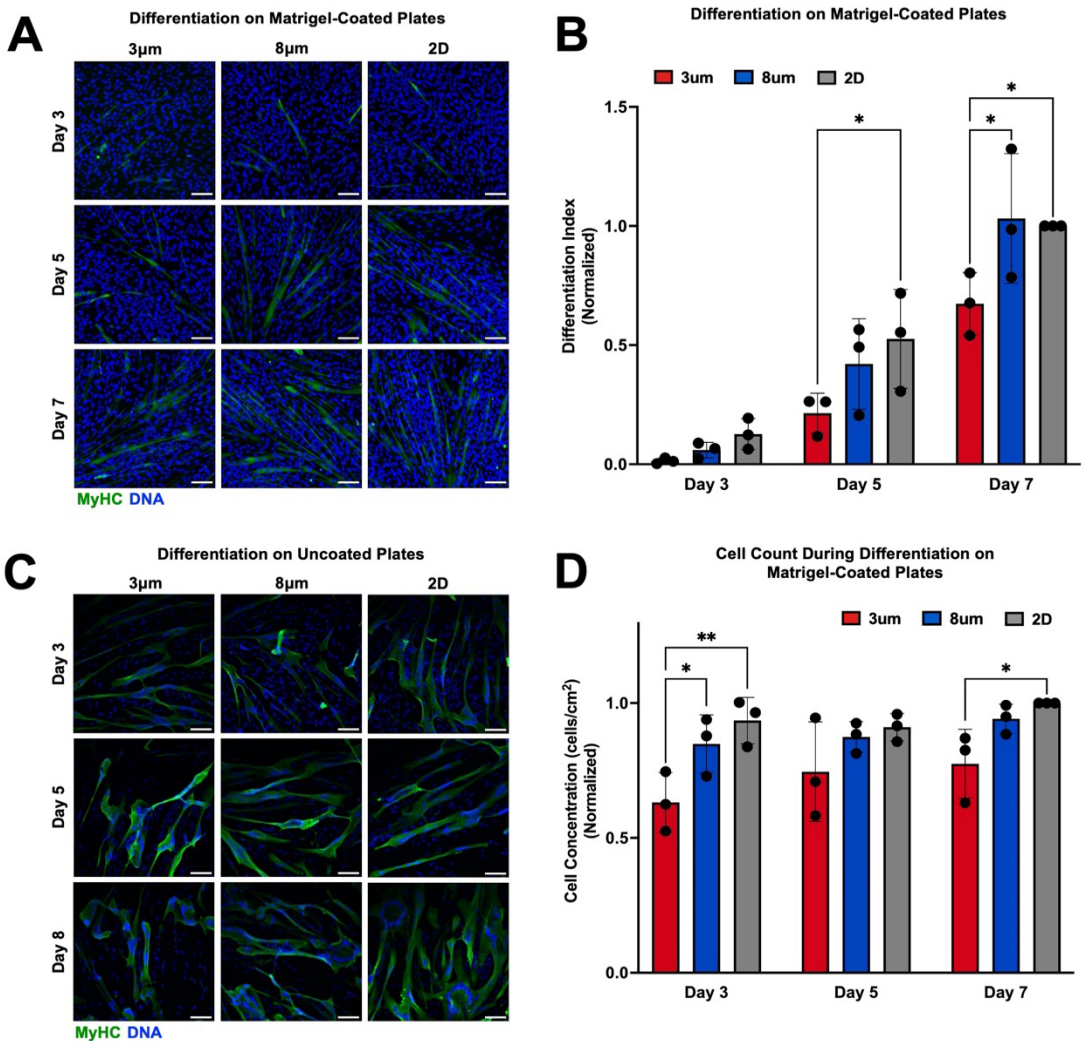

Figure 3: Differentiation of human myoblasts. (A) Representative images of cells differentiating on Matrigel-coated plates. Cells stained for myosin heavy chain (myotubes) and DNA. (B) Differentiation index at days 3, 5, and 7 for cells that underwent 3μm migration, 8μm migration, or no migration (2D). (C) Images of cells differentiation on uncoated plates. (D) Cell concentration at day 3, 5, and 7 for the 3μm, 8μm, and 2D conditions differentiating on Matrigel-coated plates. Scale bar = 100μm. * $p < 0.05$, ** $p < 0.01$

of transwell inserts after 48 hours of migration, or from the well itself for the "2D" control of cells that did not undergo transwell migration. The cells were then densely plated on Matrigel-coated plates and allowed to differentiate in serum-free medium. Plates were fixed after 3, 5, and 7 days of differentiation and immunostained, and the □ifferrentiation index was quantified.

The 3μm-migrated cells are significantly less differentiated than the unmigrated cells at days 5 and 7: the differentiation index is about 60% lower at day 5 and 33% lower at day 7 (Figure 3, A and B). Differentiation also appears to be somewhat impaired in the 3μm condition at day 3, but the differences at this early time point are too small to be statistically significant. Interestingly, the differentiation index of the 8μm-migrated cells is slightly lower, though not significantly, than that of the 2D cells at day 5, but is almost identical at day 7 (Figure 3B).

During the first attempts at these differentiation experiments, the plates were not coated with Matrigel. These experiments were unsuccessful because the myotubes began to peel off the plate as they differentiated, making accurate quantification impossible (Figure 3C). Cells also tended to form large clumps in myotubes rather than the more linear organization they take in the successful differentiation experiments, which also meant that cell density could not be calculated as nuclei could not be differentiated from one another (Figure 3, A and C).

The peeling and clumping indicated problems with adhesion, and the effect seemed the most prominent in the 3μm condition, leading us to hypothesize that constricted migration impairs cell adhesion. To further support this, cell numbers from the Matrigel-coated differentiation experiments were compared, and the 3μm condition did have significantly fewer cells than the 2D condition at 3 and 7 days of differentiation (Figure 3D). Even though the Matrigel enabled much more cell adhesion than the plates alone, there still appears to be a deficit following constricted migration.

Cell Adhesion and Spreading Decrease following Constricted Migration

After noting that adhesion appears to be impaired following constricted migration, we assessed adhesion more directly. The transwell migration process was repeated, plating cells at the

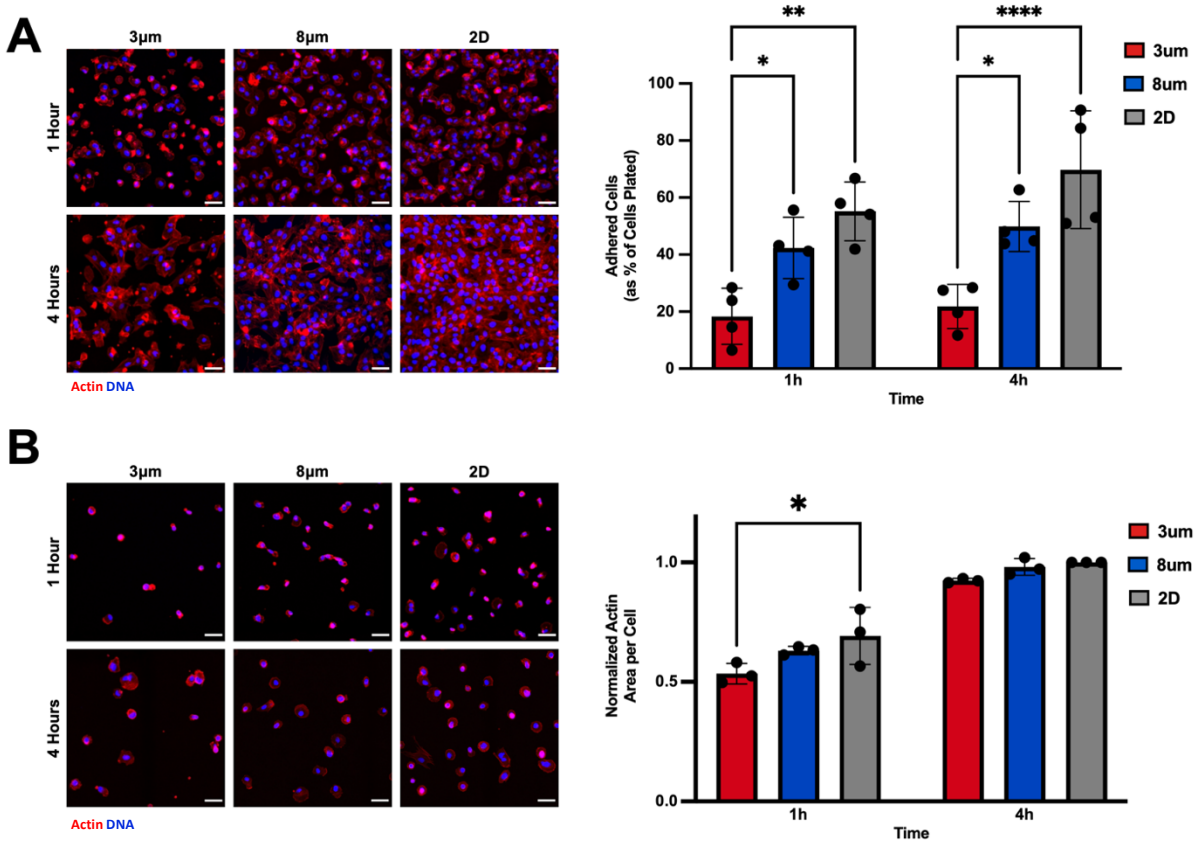

Figure 2: Myoblast adhesion and spreading. (A) Cells following migration 1 hour (top) and 4 hours (bottom) after seeding on a plate and quantification of the number of cells as a percentage of the number seeded. (B) Cells plated more sparsely 1 hour (top) and 4 hours (bottom) after seeding and quantification of the actin area per cell. Scale bar = 50μm. * $p < 0.05$, ** $p < 0.01$, **** $p < 0.0001$

same density as we did for differentiation. Cells were gently washed to remove unadhered cells, then fixed at either one hour or four hours after migration and labelled for DNA and Actin (Figure 4A and B).

The cells per area were quantified for each condition, and we found that the constricted condition had significantly fewer cells adhered than the 8μm and 2D conditions, with only about 20% of the cells initially plated remaining after both one hour and four hours. Similarly to differentiation, the number of cells in the 8μm condition was slightly lower than the 2D condition,

but not significantly.

While analyzing the images, we noted that, based on the actin signal, cells appeared more spread in the 8μm and 2D conditions than they did in the 3μm condition (Figure 4A). We attempted to quantify the actin area, but the cells were plated very densely and were overlapping so that the actin could not be differentiated between cells.

To better assess the cell spreading, we repeated the experiments with the cells plated sparsely. The actin area per cell is about 20% lower following 3μm migration than the 2D condition after one hour, and there were no differences at 4 hours, indicating an impairment of cell spreading early on that could contribute to the reduced adhesion (Figure 4, B and C).

Apoptosis and Necrosis

Our primary measure of cellular adhesion was based off of the number of cells remaining on a plate. While adhesion is likely the key contributor to the deficit following constricted migration, there may be other factors to consider such as cell death. Therefore, we attempted to measure apoptosis following constricted migration. The apoptosis and necrosis kit used to complete this assay used externalized phosphatidylserine (PS) to indicate apoptosis and loss of membrane integrity to indicate necrosis. Live cells were stained immediately following collection from the bottoms of the transwell inserts. They were imaged in suspension using a Countess slide.

We discovered that the PS indicator stained the cells in an inconsistent, punctate pattern, making it difficult to distinguish apoptotic cells from debris or nonspecific staining (Fig. 5A). After closer examination, we developed a script in FIJI to identify what we believe to be apoptotic cells with minimal bias. We tested three distinct sensitivity levels. Regardless of sensitivity, no differences were found between constricted cells and control cells (Fig. 5C).

The Nuclear Green DSC1 signal, which marks loss of nuclear integrity, was easily identified manually, so the number of necrotic cells were counted based on visual observation (Fig. 5B). The percentage of necrotic cells was significantly higher following migration through 3μm and 8μm transwells than the 2D control (Fig. 5D). Contrary to our prediction, however, there was no difference between the 3μm and 8μm conditions, with 8μm actually tending to have the most necrotic cells (Fig. 5D).

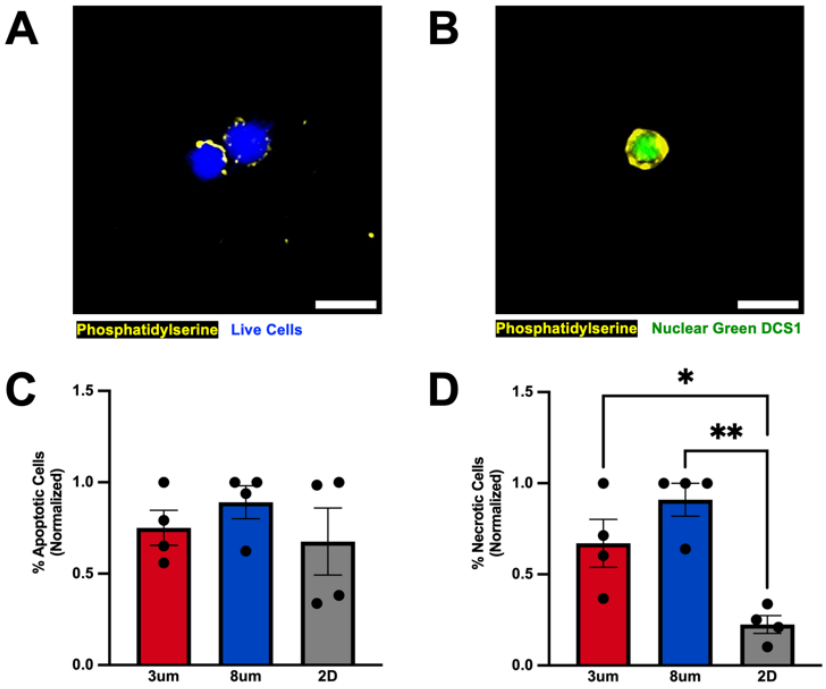

Figure 5: Apoptosis and necrosis. (A) Two live cells surrounded by punctate phosphatidylserine (PS) signal. (B) A necrotic cell surrounded by more solid PS signal. (C) Quantification of the percentage of apoptotic cells following migration. (D) Quantification of the percentage of necrotic cells following migration. Scale bar = 20μm. * $p < 0.05$, ** $p < 0.01$

Discussion

Skeletal muscle regeneration is dependent on muscle satellite cell differentiation and fusion [4,40]. As mechanosensitive cells that interact closely with their surrounding microenvironment, it is conceivable that satellite cell fate is influenced by the changes in the extracellular matrix that occur during chronic muscle fibrosis [41,42].

Due to their location on the periphery of myofibers before activation, satellite cells must

migrate to the site of an injury to repair the myofiber [23,25]. Fibrosis is marked by an increase in collagen content and collagen crosslinking which leads to a matrix that is more dense and more difficult to remodel [43]. As a result, we propose that satellite cells undergo migration through tight pores that constrict their nuclei more frequently in fibrotic muscle than healthy muscle. In this study, we utilize human myoblasts to explore the effects of constricted migration on muscle progenitors.

The results of constricted migration on the human myoblast cell line used in this study align well with the effects observed in a mouse myoblast cell line in a previous study [21]. In both cases, the cells exhibited increased DNA damage and impaired differentiation [21]. Certain effects are more pronounced in human cells than in mouse cells, such as nuclear blebbing, where over 80% of human myoblasts have blebs following 3μm migration compared to about 30% of mouse myoblasts [21]. In addition, mouse myoblasts do not demonstrate a severe adhesion deficit following constricted migration; they can typically be differentiated on uncoated plastic without issue, while human myoblasts require coating with proteins to increase adhesion.

There are a few possible means through which constricted migration may impair differentiation. Along with inducing DNA damage, nuclear rupture can cause mislocation of nuclear proteins and transcription factors [21,32]. This includes MyoD, a myogenic regulatory factor, as well as KU80, a DNA damage repair factor, both of which have been identified as important to myogenic differentiation [21,22,44]. Future experiments can use immunohistochemistry to confirm whether mislocalization of DNA repair factors occurs. Higher levels of DNA damage that does not get repaired well can lead to problems such as cell death and genomic instability, which may further impair satellite cell function [37].

DNA damage has also been found to limit myogenesis in mouse myoblasts by inhibiting

MyoD, which halts the cell cycle, preventing differentiation [45]. This effect is reversible upon removal of the source of damage [45]. This response may occur in human myoblasts that undergo extensive DNA damage from 3μm constricted migration causing them to be unable to differentiate until the damage is repaired, leading to delayed differentiation compared to cells without damage. Evidence was also found indicating that sustained damage can lead to abnormal muscle cells [45]. Thus, persistent damage incurred while migrating through a fibrotic matrix could contribute to the weakness of freshly regenerated muscle fibers in muscular dystrophy.

Another factor that may contribute to impaired myoblast function is the apparent adhesion deficit following constricted migration. When attempting to differentiate human myoblasts on tissue-culture plastic, they did not adhere well to the plates. This effect was the most pronounced following 3μm migration, leading us to propose that adhesion may be negatively impacted by constricted migration. These effects were mitigated by culturing the cells on Matrigel-coated plates, but we decided to explore the deficit on plastic further and saw that indeed, at early time points, significantly fewer cells were attached to the plate in the 3μm condition than the control "2D" condition.

Because these measurements were taken at 1 and 4 hours after seeding, it is highly unlikely that the differences in the number of cells were due to proliferation, which occurs on a longer time scale, about 40 hours in normal growth conditions. This could be confirmed in future experiments using an Edu proliferation assay, or proliferation could be delayed by modifying cells to overexpress myostatin [64]. On the other hand, apoptosis can occur more quickly, so we attempted to quantify apoptosis following constricted migration.

The apoptosis and necrosis kit-stained phosphatidylserine on the exterior of cells to indicate apoptosis and used loss of nuclear integrity for necrosis. While we were not able to identify

differences in the overall rate of apoptosis, we did see an increase in necrosis following migration. In other experiments, even when there was no significant difference between the 3μm and 8μm conditions, the 8μm tended to be similar to the 2D control, or somewhere in the middle of 3μm and 2D. We did not see such an effect in this experiment; in fact, the 8μm mean tended to be slightly higher than 3μm, though not significantly. This may indicate that transwell migration promotes necrosis in human myoblasts, but not constricted migration specifically. It is possible, therefore, that necrosis contributes to the differences in the number of cells attached to plastic after 1 and 4 hours.

We encountered a number of challenges with the apoptosis kit used in this study; initial flow cytometry assays did not demonstrate clear population differences, and fluorescent imaging revealed debris and irregular, punctate staining. In future studies, we recommend utilizing an alternate apoptosis detection method such as the TUNEL assay.

There are likely other factors contributing because there were significant differences between the 3μm and 8μm conditions observed in the adhesion assay that were not present in the necrosis assay, meaning that necrosis does not fully explain the deficit. We attempted to quantify cell spreading by repeating the adhesion assay with a lower cell density so individual cells could be observed without overlap. At 1 hour after seeding, the average actin area per cell was lower following 3μm condition than it was in the 2D control. The effect was small, but statistically significant.

Qualitatively, there seems to be a larger difference in cell spreading in the higher-density experiments. The effect may have been reduced in the lower-density experiment due to limited cell-cell signaling between the sparsely plated cells. Aside from being influenced by cell density, cell spreading may also be affected by damage to cellular components that affect adhesion, such

as surface proteins involved in forming focal adhesions. Cell concentration, adhesion, and spreading are all closely interconnected processes, so it's difficult to fully isolate one component.

These factors all play important roles in myogenesis, so if they are inhibited following constricted migration, the cells may exhibit impaired differentiation [46–48]. Despite seeding cells at a consistent density and coating tissue culture wells with Matrigel to improve adhesion, fewer cells remained on the Matrigel-coated plates after 3 and 7 days of differentiation in the 3μm condition than in the 2D condition. Therefore, the persistent difference in cell numbers may affect differentiation. However, as discussed above, there are a number of other potential players in the differentiation deficit, so it is unclear what specific consequence of constricted migration causes the deficit.

Effective muscle regeneration depends on the synergy of multiple cell types, including muscle satellite cells, fibroblasts and fibroadipogenic progenitors, and immune cells [40,49]. When any of these cell types doesn't function as intended, it has detrimental implications for muscle repair. For example, ablation of fibroblasts causes early differentiation of satellite cells and reduced myofiber size after injury [40]. Correspondingly, the infiltration of a variety of cell types to coordinate regeneration in muscle may each be exposed to constricted migration that impacts their support of MuSC regeneration.

The present study makes the assumption that myoblasts undergo constricted migration in fibrotic muscle. This has not yet been proven, and there is evidence that collagen may be less densely packed in fibrotic muscle ECM which could indicate that constricted migration is no more likely in fibrotic muscle than in healthy muscle [50]. However, it is widely accepted that constricted migration occurs during cancer metastasis, so it is not unreasonable to suspect that it also occurs during the migration of other cell types *in vivo* [31,33].

Another consideration in assessing this study is the relevance of transwell inserts as a model of cellular migration. Unlike migration *in vivo,* transwell migration occurs only in one dimension, through hard plastic, so it may not accurately capture the motions of cells in a 3D environment. Transwell experiments may be adapted to better mimic the *in vivo* environment, such as by adding ECM for cells to remodel or by including a growth factor gradient, which is especially relevant in muscle, where soluble signals activate muscle satellite cells and direct their migration. Additionally, alternatives such as microfluidic devices designed to model constricted migration can allow cells to move in a more physiological manner. Such devices have been developed for future work on this topic.

A final note on the transwell assays is the variation in cell concentration between experiment types. To optimize time and cell usage, the concentration of cells/cm^2 was lower for the experiments using 6-well inserts (differentiation, adhesion, and apoptosis) than it was for those using 24-well inserts. This introduces an additional confounding variable that weakens the ability to compare the experiments. In future work, the same cell concentration will be utilized for all transwell experiments to eliminate this inconsistency.

There is a myriad of factors that contribute to the secondary effects of diseases like muscular dystrophy, many of which have yet to be identified. Identifying and understanding some of these factors may present a novel treatment approach. We propose that constricted migration of muscle satellite cells occurs as a consequence of the dense fibrotic extracellular matrix which, in pathogenic states, is not as easily remodeled by cells to allow them to migrate through larger spaces and minimize constriction. We found that constricted migration through 3μm-diameter pores induces high levels of nuclear rupture in human myoblasts, which causes DNA damage, impaired adhesion, and impaired differentiation. Therefore, we conclude that constricted migration may be

responsible, in part, for muscle satellite cell deficits observed in muscular dystrophy patients. This can also provide new targets for treatment. Blebbistatin, for example, minimizes nuclear rupture during constricted migration, which could minimize DNA damage incurred following muscle injury, though it does also greatly reduce migration rates [21]. Treatments can also focus on improving the ability of satellite cells to remodel their local microenvironment. Satellite cells may be genetically transformed to overexpress matrix metalloproteinases or reduce expression of tissue inhibitors of metalloproteinases (TIMPs).

Satellite cell function is vital for the successful regeneration of muscle following injury. Thus, it is important to focus on factors that may impede satellite cell function in muscular dystrophy, which is characterized by repeated injury and fibrosis. Improving muscle regeneration can reduce the recurrence of injuries, thus slowing the positive feedback loop of fibrosis, poor regeneration, and injury.

Chapter 3. 3D Culture of Human Myoblasts

Introduction

Traditional assays utilized to study satellite cells *in vitro* require culturing the cells on plastic, which is sometimes coated with extracellular matrix (ECM) components, or gels containing these components, to improve cell adhesion and survival. While two-dimensional culture is straightforward and useful for many studies, it does not effectively mimic the complex physiological environment with which cells interact *in vivo.* There are many efforts to improve the physiological relevance of cell culture, most of which focus on three-dimensional cell culture and tissue engineering.

Tissue-engineered skeletal muscle can be used to study muscle biology as well as for drug discovery and screening [51]. Beyond its use in research, engineered muscle could even be implanted as therapeutic endogenous muscle grafts [51]. Skeletal muscle is a complex and dynamic tissue, making it both challenging and important to accurately mimic *in vitro.* There are many considerations that go into developing engineered muscle tissue and selecting which aspects of physiological muscle to recreate. Some factors include vascularization, innervation, mechanical or electrical stimulation, co-culture with associated cell types, and any other characteristic or component of the *in vivo* muscle microenvironment [52,53].

The ECM is a key element in the vast majority of engineered muscle. The ECM facilitates cell adhesion, provides a physical scaffold and structural support, improves force transmission, and enables the cells to remodel their local microenvironment [29,54]. Collagen I, the most abundant protein in muscle ECM, is one important ECM protein. Cells can be cultured in 3D collagen hydrogels, resulting in larger myotubes than cells cultured on a flat surface [54]. The concentration, crosslinking, and alignment of collagen gels can be modified to further influence

cell behavior and the structure of the resulting tissue [29,54,55]. However, collagen I may not be the optimal basis for microtissues, resulting in less robust microtissues and lower force generation than an alternate ECM-based gel using fibrin [29]. This may be in part because the collagen I gels are stiff, potentially mimicking a fibrotic environment and therefore impairing differentiation [28,29,54]. Fibrin is another ECM protein that is useful for engineering muscle. Though it isn't abundant in native muscle, it is a transient protein that is more easily remodeled by cells than collagen, and fibrin gels have a lower stiffness that aligns with native muscle ECM [54,56,57]. Fibrin concentration affects the characteristics of engineered muscle microtissues, with higher concentrations leading to increased cellular hypertrophy and force generation [29].

Matrigel, a gel formed from an extract of the basal lamina of a murine tumor, is also widely used for tissue engineering. In muscle, myotubes interact directly with the basal lamina, so Matrigel helps mimic these direct interactions more accurately, improving cellular adhesion and myotube formation [29]. Matrigel consists of ECM proteins such as laminin, collagen IV, and entactin – which are present in the muscle ECM as well – along with a variety of growth factors; growth factor-reduced Matrigel is also available to reduce confounding variables [58,59].

This study aims to adapt an engineered microtissue or "myobundle" design – which uses a fibrin/Matrigel matrix to culture primary satellite cells in a PDMS mold – for a human myoblast cell line [54,60]. Myoblast cell lines proliferate more readily than primary cells, and therefore larger sample sizes can be used to test a variety of conditions, while also minimizing variability. They are also more accessible and can be obtained and cultured in greater quantities. On the other hand, they can be limited in their ability to behave in a way that mimics satellite cell behavior *in vivo,* which is the key advantage of primary cells. Such a design can be customized by using different ECM proteins in varying concentrations to mimic features of diseased muscle such as

chronic fibrosis. Alternately, cell concentration can be modified to mirror reduced proliferation, or cells can be used following damage-inducing treatments such as constricted migration. This study details the development of the device and early experiments that validate the potential to study a myoblast cell line with this technique.

Methods

Preparation of Devices

The mold master for the three-dimensional cell culture platform was developed using AutoCAD and printed using stereolithography (SLA) 3D printing, which was selected due to its high accuracy and resolution. Early prototypes were printed with lower resolution, leading to topography that could influence cell behavior. The mold was designed with two identical "dumbbell" shapes, where the main channel was just over half of a cylinder with a radius of 1.375mm and a length of 6.4mm, and the rectangular depressions at either end of the channel had a depth of 1.5mm, length of 2mm, and width of 4.5mm (Fig 6C). The mold master was designed with rounded edges to reduce bubble formation in the PDMS, as bubbles tended to accumulate around the sharp corners of the earlier prototype (Fig 6, A and B).

6-well plates were used to create the molds. First, liquid polydimethylsiloxane (PDMS) (Sylgard 184), was slowly poured into each well to cover the surface, then was cured overnight in an oven at 37°C to create a base layer of PDMS so the bottom of the mold doesn't touch the plate. The next day, fresh PDMS was prepared, and poured slowly around the mold master to reduce bubble formation. The PDMS was again cured at 37°C overnight, and the mold masters were removed the next day. If bubbles did form, the mold master was manipulated with forceps to allow them to escape, or to move them to the edges of the well where they would not interfere with the microtissue. Finally, Velcro was cut into rectangles to fit in the depressions at either end of the

main channel, and attached with a small amount of PDMS that again was cured overnight.

Devices were sterilized in the aseptic biosafety cabinet (BSC) using ethanol, which was poured to cover the entire well. The ethanol was left on for 30 minutes, and the UV light in the BSC was turned on. The ethanol was aspirated and the PDMS was allowed to dry, then the channels were coated with Pluronic F-127 to inhibit cell adhesion to the PDMS. 0.2% Pluronic

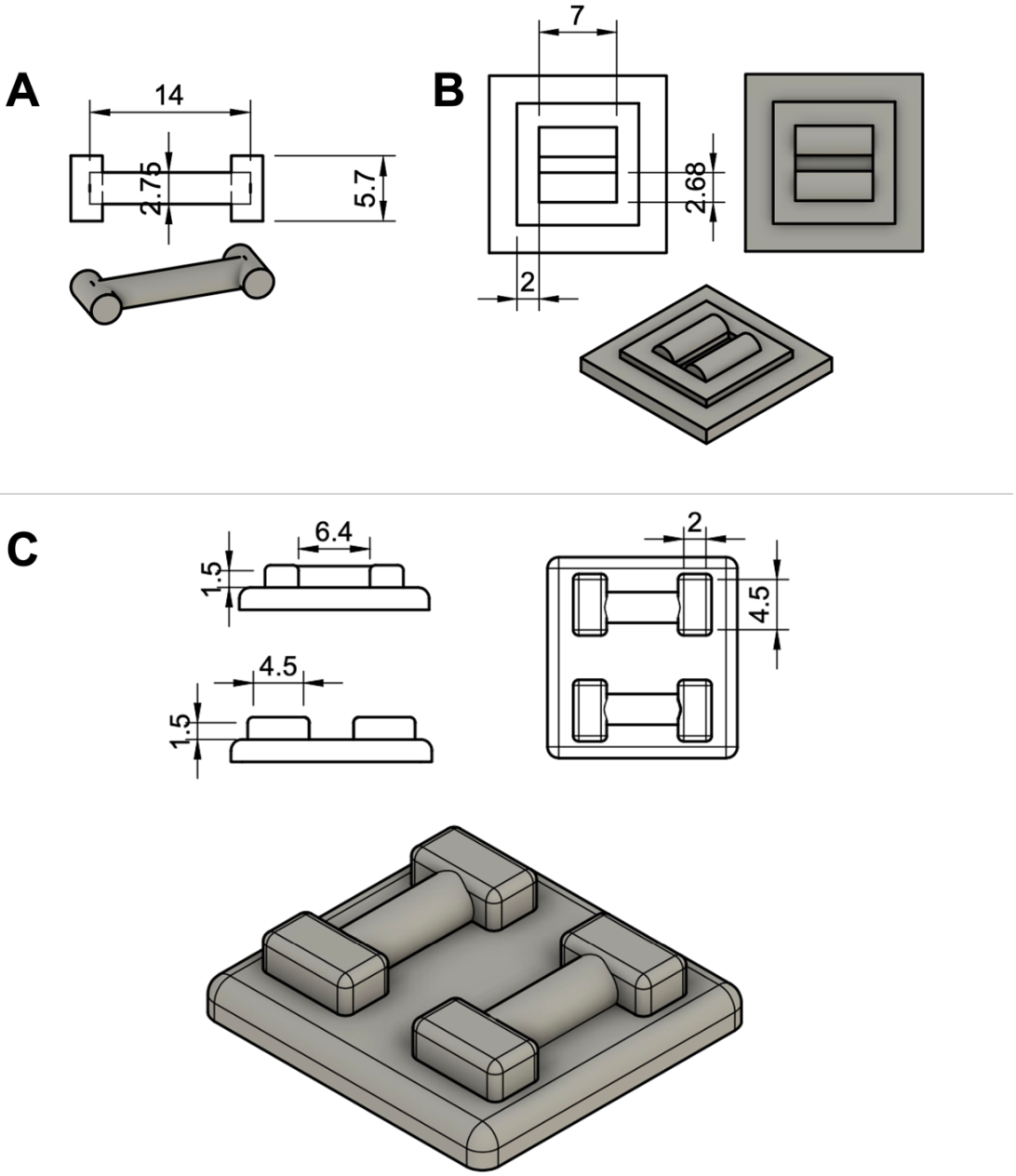

Figure 6: Diagrams of iterations of mold design on Fusion 360. (A) Initial model, single "dumbbell". (B) Second model with two "dumbbells" per device. (C) Final model with curved edges and increased separation between channels.

was left in the channels for 30 minutes, then aspirated and washed twice with PBS. The plates were sealed with Parafilm until the start of the experiment.

Plating Cells

The gelling solution was prepared first, consisting of 20 mg/mL fibrinogen dissolved in DMEM, human myoblast growth media (HGM), and Matrigel, at a 1:1:1 proportion. This solution was left in the fridge at 4°C until it was ready to be used to ensure the Matrigel did not begin to gel at room temperature.

The cell solution included cells, thrombin, and HGM. A 10μL aliquot of thrombin (prepared at a concentration of 100 units/mL) was combined with 10μL of HGM for a concentration of 50 units/mL. Cells were removed from the plate using trypsin, spun down in the centrifuge (300g for 5 minutes at 4°C), and resuspended in HGM at a concentration of approximately 3×10^7 cells/mL. 172μL of the resuspended cells was combined with 20μL of the diluted thrombin. Because of the very high number of cells used, another experiment was performed following the same procedure but using the following cell concentrations: 3×10^7 cells/mL, 1.5×10^7 cells/mL, 3×10^6 cells/mL, or 1.5×10^6 cells/mL.

The cell solution was distributed into 19.2μL aliquots. One at a time, 31μL of the gelling solution was added to an aliquot. They were mixed by pipetting up and down quickly, and then the whole volume was pipetted into one myobundle mold, taking care to minimize bubbles and ensure the solution was in contact with the Velcro as well as the mold itself. The plate was placed back in the incubator for 30 minutes to help the gel polymerize, then 2mg/mL 6-aminocaproic acid (6-ACA) growth media was added to cover the wells. Two days later, the GM was replaced with 2mg/mL 6-ACA differentiation medium, which was changed every 2-3 days for as long as the myobundles were cultured. During the cell concentration experiment, the plate was photographed

occasionally to track macroscale myobundle formation. All myobundles were fixed with 4% paraformaldehyde prior to immunostaining, which was performed as described in the prior chapter.

Results

Myobundle Formation

The myobundles were cultured for two weeks, and the cells successfully differentiated (Fig. 7A). Some of the wells did not successfully form myobundles, indicating the sensitivity of this procedure. They were very sensitive to air bubbles during seeding which, due to the small size of the myobundles, left a relatively large void where the bubble was. If the Velcro was not adequately covered, the myobundles either did not form or they began to form but detached from the Velcro early on.

At concentrations of 3×10^7 and 1.5×10^7 cells/mL, robust myobundles quickly began to develop (Table 1). At lower concentrations of 3×10^6 and 1.5×10^6 cells/mL, the cells did not differentiate as readily. The lowest concentration did not form myobundles at all; i.e. there was no compaction or remodeling of the matrix. The 3×10^6 gels formed weak myobundles that did not compact as much as the higher concentrations. Visually, these weaker myobundles had a more translucent appearance. When gently handling them, they lacked structure and fell apart easily (Fig. 7A). In contrast, the more robust myobundles appeared more opaque and could be easily handled while maintaining their shape.

To attempt to quantify the observed differences in myobundle compaction, the width of each myobundle at its smallest point was estimated over time. Pictures were taken of the plate at the time points of interest, and FIJI was used to estimate the width, using a nearby feature of the mold to set the scale for each myobundle. The 1.5×10^6 myobundles were excluded from this analysis as there was no compaction. Both the 1.5×10^7 and 3×10^6 myobundles decreased in width throughout

the length of the experiment as the cells remodeled the ECM and continued to differentiate, and the 1.5×10^7 bundles were indeed more compact than the 3×10^6 (Fig. 7B). Interestingly, the 3×10^7

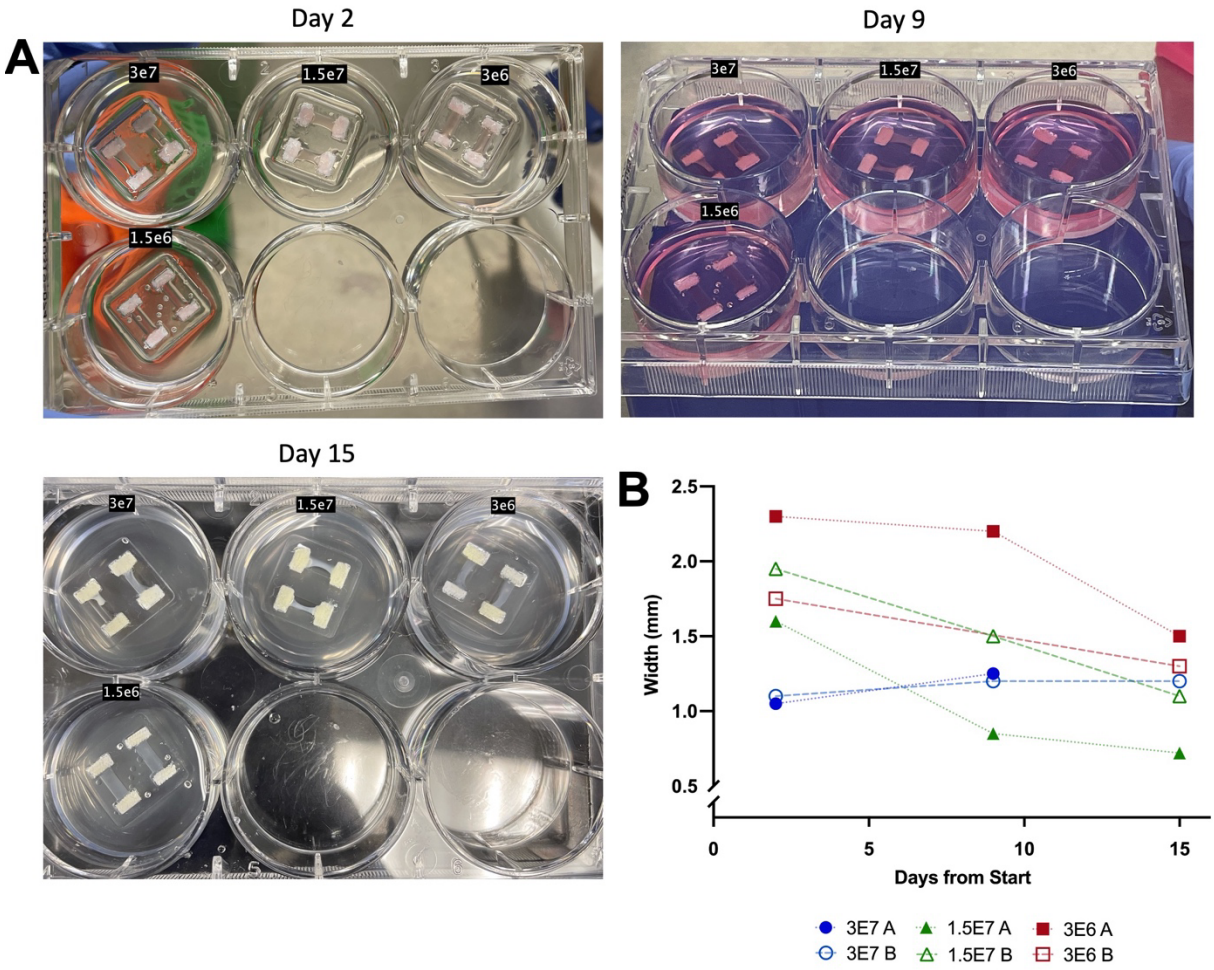

Figure 7: Myobundle compaction. (A) Pictures of microtissues over time. (B) Approximate quantification of myobundle width over time at their smallest point.

myobundles were the most compact at the beginning but did not compact further with more time. One of these bundles was poorly attached at the beginning, detached partially by the second time point and completely by the third, likely due to an error loading the molds (Fig. 7A). The surviving bundle was less compacted than both 1.5×10^7 myobundles at the third and final timepoint (Fig. 7B). This semi-quantitative analysis demonstrates that cells in myobundles with a higher cell concentration remodel their surrounding ECM to a greater degree than lower cell concentrations,

but points to an optimal concentration that may be below the highest concentration tested.

Table 1: Qualitative assessment of myobundle formation given different cell concentrations.

Initial Cell Concentration (cells/mL)	Cells per Myobundle	Cell Concentration in Myobundle (cells/mL)	Myobundle Quality
3×10^7	2.69×10^6	5.35×10^4	Robust
1.5×10^7	1.34×10^6	2.68×10^4	Robust
3×10^6	2.69×10^5	5.35×10^3	Fragile
1.5×10^6	1.34×10^5	2.68×10^3	No Myobundle

Myotubes and Alignment

After fixation, myobundles were stained to visualize cell alignment and differentiation. The first set of myobundles, which were cultured for two weeks, had very clear myotubes, identified by myosin heavy chain (Fig. 8A). The myotubes were well-aligned longitudinally along the myobundle length. Most myotubes had a few nuclei within them, but it appeared that there were still many nuclei that were not fused in myotubes. Some of the unfused nuclei were elongated and aligned in the same direction as the myotubes, while others remained round and didn't exhibit any notable alignment.

The myobundles used to test different cell concentrations were cultured for a few days longer than the initial myobundles. Some of them seemed to adhere to the PDMS mold at points, leading to uneven compaction. The 1.5×10^6 myobundles lacked structural integrity and could not handle being manipulated in an attempt to image them. The 3×10^6 bundles were also fragile, so they were imaged while still in the mold (Fig. 8B). This made the images blurrier, but it was possible to ascertain that there was some MHC signal surrounding individual nuclei, and it seemed like there was minimal, if any, fusion or myotubes. There was also no notable alignment. The two well-formed myotube conditions were removed from the molds and imaged on coverslips. In both cases, the nuclei and myosin heavy chain signal demonstrate some alignment, though the myotubes were

fairly thin and did not seem to encompass many nuclei.

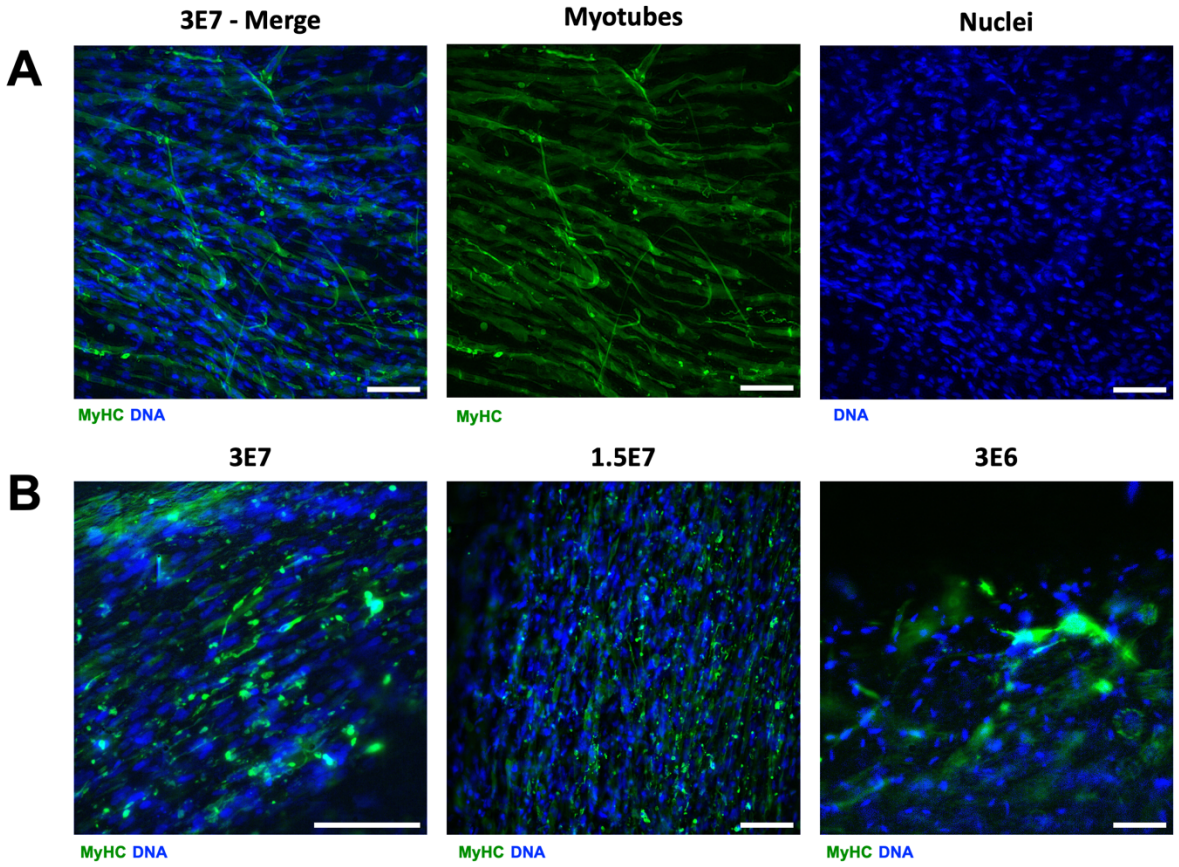

Figure 8: Fluorescent imaging of microtissues. (A) Image of the first microtissue at 2 weeks, demonstrating aligned myotubes. (B) Images of microtissues with varying cell concentrations at 15 days showing different levels of differentiation and alignment. Scale bar = 100μm.

Discussion

Three-dimensional cell culture and tissue engineering are useful tools to replicate a physiological environment to more accurately study cell behavior *in vitro.* It is more cost-effective, more controllable, and simpler to analyze cell behavior in engineered tissues than it is *in vivo*. In particular, studying cell behavior in real time *in vivo* requires obtaining or breeding transgenic mice to express fluorescent proteins and using intravital imaging to visualize changes over time [25]. Engineered muscle can provide an alternative; cells can be genetically transformed to express any number of fluorescent proteins, and engineered muscle developed from these cells can be imaged at any point without specialized equipment.

The device presented in this study utilizes extracellular matrix (ECM) proteins to develop muscle microtissues from immortalized human myoblasts. The design was based on the model published by Hinds et al. in 2011 [29]. The authors utilized primary neonatal rat skeletal myoblasts with fibrin/Matrigel hydrogels, as well as collagen/Matrigel hydrogels. The cells did not differentiate as well in the collagen-based gels, so the fibrin-based gel was used in the subsequent studies and further development of the model by the Bursac Lab. Because the microtissue method was developed using primary cells, which tend to differentiate very readily, the fibrin-based gel was selected for the early studies of the human myoblast cell line to facilitate the successful formation of myobundles.

The majority of engineered muscle tissue utilizes primary satellite cells as the cell source, but transformed cell lines such as C2C12 mouse myoblasts can also form 3D tissue capable of spontaneous contraction using another fibrin gel-based method [61]. Based on this proof of concept, the observation in this study that well-differentiated myotubes developed from immortalized human myoblasts was expected. The myobundles resulting from this method, however, did not exhibit spontaneous or induced contraction, so the technique requires further optimization.

There is also conflicting evidence based on a similar method that suggests C2C12 cells do not differentiate well on fibrin-based hydrogels, but instead require collagen for effective microtissue formation [62]. Future studies of the present device should compare a collagen/Matrigel mixture to the fibrin/Matrigel mixture. Utilizing collagen as the basis of the microtissue can be useful for many reasons aside from potentially improving differentiation. Fibrin is not abundant in the healthy muscle ECM, meaning it is not particularly physiological in terms of replicating the muscle microenvironment. Collagen, on the other hand, is one of the primary components of the muscle

ECM [29]. Fibrin is, however, a key component of the transitional matrix deposited following muscle injury [11]. As such, it is easily remodeled, which makes it useful as a scaffold but adds the additional challenge of preventing cells from fully degrading the matrix, though this can be overcome by using fibrinolysis inhibitors such as 6-ACA, demonstrated by its use in the present study to limit degradation of the fibrin-based hydrogel [54].

Collagen presents its own challenges; primarily, it is stiff and not easily remodeled by cells, leading to limited force generation [63]. The stiffness and high collagen content may inadvertently cause collagen-based gels to mimic a fibrotic environment. While this is not the goal of most engineered muscle tissues, it does mean that collagen can be a useful tool to model a diseased muscle state. Chronic muscle fibrosis occurs in a number of diseases, so customizing engineered tissues to recapitulate the fibrotic microenvironment *in vitro* by modifying collagen content, the availability of matrix metalloproteinases (MMPs) and tissue inhibitors of metalloproteinases (TIMPs), stiffness, or other features can greatly improve studies of pathologic cell behavior.

In addition to modeling a fibrotic environment, microtissues can be grown from cells that have undergone damage similar to that which they may face in pathologic muscle, such as constricted migration. Engineered muscle can be used as an alternative measure of cellular function – in place of differentiating cells on a plate, where they tend not to adhere well even with ECM coatings, they could be differentiated in a more physiological 3D environment built from native ECM proteins (Fig 2C). This can facilitate better differentiation and may reduce disparities between treated cell populations due to adhesion deficits. It can also provide additional functional measurements by quantifying force generation or other qualities, which is especially beneficial as differentiation and fusion alone do not necessarily tell the whole story of the regenerative capacity of cells. The microtissues developed in this study can provide novel approaches to probe the

importance of ECM content and architecture to satellite cell behavior in an environment more closely related to muscle.

4. Conclusions

This thesis concludes that human myoblasts demonstrate adhesion and differentiation deficits following constricted migration. These deficits likely arise from the high levels of nuclear rupture that were found to occur following migration through 3μm-diameter pores, which is the most probable source of the increased DNA damage also observed in these cells. This builds upon prior work performed using a mouse myoblast cell line, demonstrating that the effects of constricted migration are similar in the more relevant human myoblast cell line, and may even be exaggerated, as is the case for nuclear rupture. We suggest that these results can explain, in part, the impaired regenerative function of muscle satellite cells that is observed in Duchenne muscular dystrophy patients.

There are two key limitations of this study that should be explored in future work. First, the motivation for the research should be validated by determining whether constricted migration happens to muscle stem cells *in vivo.* This could be achieved using immunohistochemistry to identify signs of nuclear rupture in fibrotic and healthy muscle tissue, or by using intravital imaging to track muscle stem cell behavior in real time and provide a more complete picture of their migration [25]. Second, the mechanisms behind changes in myoblast behavior should be further elucidated. Immunocytochemistry can be used to identify different myogenic and DNA repair factors and determine whether they are mislocated following constricted migration. Another method could be to use RNA sequencing to explore differences in gene expression between myoblasts that have undergone constricted migration or cells that haven't; it could also be used to compare freshly isolated muscle satellite cells from healthy and fibrotic animals.

The thesis also presents a method to develop 3D muscle microtissues with the same human myoblast cell line. These microtissues can improve *in vitro* studies of diseases like DMD by providing a customizable extracellular matrix base that can be used with immortalized cells, which have greatly reduced variability in comparison to primary satellite cells and are more easily accessible. Future work with this device should include further optimization of cell number, media, and hydrogel makeup so that the cells are able to differentiate more completely and more closely model *in vivo* myotubes, including having the ability to contract.

Future studies can also continue to develop the device with different substrates to model fibrosis by varying collagen content. They can also be used to provide an alternative method to measure cellular function following constricted migration, with increased physiologic relevance based on the fibrin (or collagen) and Matrigel matrix and measurements of force generation. This could also minimize or eliminate the effects of factors such as reduced adhesion that made it more difficult to accurately measure differentiation.

Together, these results motivate and demonstrate the potential for further studies of constricted migration and the effect of a fibrotic environment on myoblast behavior. These studies can better replicate the complexities of muscle and improve understanding of pathologies such as DMD, ultimately providing new targets for therapies.

References

1. Schmidt, M., Schüler, S.C., Hüttner, S.S., von Eyss, B., and von Maltzahn, J. (2019). Adult stem cells at work: regenerating skeletal muscle. Cellular and Molecular Life Sciences *76*, 2559–2570. 10.1007/s00018-019-03093-6.
2. Wagers, A.J., and Conboy, I.M. (2005). Cellular and molecular signatures of muscle regeneration: Current concepts and controversies in adult myogenesis. Cell *122*, 659–667. 10.1016/j.cell.2005.08.021.
3. Dumont, N.A., Bentzinger, C.F., Sincennes, M.C., and Rudnicki, M.A. (2015). Satellite cells and skeletal muscle regeneration. Compr Physiol *5*, 1027–1059. 10.1002/cphy.c140068.
4. Relaix, F., and Zammit, P.S. (2012). Satellite cells are essential for skeletal muscle regeneration: The cell on the edge returns centre stage. Development (Cambridge) *139*, 2845–2856. 10.1242/dev.069088.
5. Hill, M., Wernig, A., and Goldspink, G. (2003). Muscle satellite (stem) cell activation during local tissue injury and repair. J Anat *203*, 89–99. 10.1046/j.1469-7580.2003.00195.x.
6. Ryder, S., Leadley, R.M., Armstrong, N., Westwood, M., de Kock, S., Butt, T., Jain, M., and Kleijnen, J. (2017). The burden, epidemiology, costs and treatment for Duchenne muscular dystrophy: An evidence review. Orphanet J Rare Dis *12*, 1–21. 10.1186/s13023-017-0631-3.
7. Mercuri, E., Bönnemann, C.G., and Muntoni, F. (2019). Muscular dystrophies. The Lancet *394*, 2025–2038. 10.1016/S0140-6736(19)32910-1.
8. Duan, D., Goemans, N., Takeda, S., Mercuri, E., and Aartsma-Rus, A. (2021). Duchenne muscular dystrophy. Nat Rev Dis Primers *7*, 13. 10.1038/s41572-021-00248-3.
9. Morgan, J.E., and Zammit, P.S. (2010). Direct effects of the pathogenic mutation on satellite cell function in muscular dystrophy. Exp Cell Res *316*, 3100–3108. 10.1016/j.yexcr.2010.05.014.
10. Ribeiro, A.F., Souza, L.S., Almeida, C.F., Ishiba, R., Fernandes, S.A., Guerrieri, D.A., Santos, A.L.F., Onofre-Oliveira, P.C.G., and Vainzof, M. (2019). Muscle satellite cells and impaired late stage regeneration in different murine models for muscular dystrophies. Sci Rep *9*, 1–11. 10.1038/s41598-019-48156-7.
11. Mann, C.J., Perdiguero, E., Kharraz, Y., Aguilar, S., Pessina, P., Serrano, A.L., and Muñoz-Cánoves, P. (2011). Aberrant repair and fibrosis development in skeletal muscle. Skelet Muscle *1*, 1–20. 10.1186/2044-5040-1-21.
12. Yanay, N., Rabie, M., and Nevo, Y. (2020). Impaired Regeneration in Dystrophic Muscle—New Target for Therapy. Front Mol Neurosci *13*, 1–12. 10.3389/fnmol.2020.00069.
13. Urciuolo, A., Quarta, M., Morbidoni, V., Gattazzo, F., Molon, S., Grumati, P., Montemurro, F., Tedesco, F.S., Blaauw, B., Cossu, G., *et al.* (2013). Collagen VI regulates satellite cell self-renewal and muscle regeneration. Nat Commun *4*. 10.1038/ncomms2964.
14. Blau, H.M., Webster, C., and Pavlath, G.K. (1983). Defective myoblasts identified in Duchenne muscular dystrophy. Proc Natl Acad Sci U S A *80*, 4856–4860. 10.1073/pnas.80.15.4856.

15. Schmidt, W.M., Uddin, M.H., Dysek, S., Moser-Thier, K., Pirker, C., Höger, H., Ambros, I.M., Ambros, P.F., Berger, W., and Bittner, R.E. (2011). DNA damage, somatic aneuploidy, and malignant sarcoma susceptibility in muscular dystrophies. PLoS Genet *7*. 10.1371/journal.pgen.1002042.
16. Boldrin, L., Zammit, P.S., and Morgan, J.E. (2015). Satellite cells from dystrophic muscle retain regenerative capacity. Stem Cell Res *14*, 20–29. 10.1016/j.scr.2014.10.007.
17. Pakshir, P., and Hinz, B. (2018). The big five in fibrosis: Macrophages, myofibroblasts, matrix, mechanics, and miscommunication. Matrix Biology *68–69*, 81–93. 10.1016/j.matbio.2018.01.019.
18. Smith, L.R., and Barton, E.R. (2018). Regulation of fibrosis in muscular dystrophy. Matrix Biology *68–69*, 602–615. 10.1016/j.matbio.2018.01.014.
19. Desguerre, I., Mayer, M., Leturcq, F., Barbet, J.P., Gherardi, R.K., and Christov, C. (2009). Endomysial fibrosis in duchenne muscular dystrophy: A marker of poor outcome associated with macrophage alternative activation. J Neuropathol Exp Neurol *68*, 762–773. 10.1097/NEN.0b013e3181aa31c2.
20. Klingler, W., Jurkat-Rott, K., Lehmann-Horn, F., and Schleip, R. (2012). The role of fibrosis in Duchenne muscular dystrophy. Acta Myologica *31*, 184–195.
21. Smith, L.R., Irianto, J., Xia, Y., Pfeifer, C.R., and Discher, D.E. (2019). Constricted migration modulates stem cell differentiation. Mol Biol Cell *30*, 1985–1999. 10.1091/mbc.E19-02-0090.
22. Yin, H., Price, F., and Rudnicki, M.A. (2013). Satellite cells and the muscle stem cell niche. Physiol Rev *93*, 23–67. 10.1152/physrev.00043.2011.
23. Siegel, A.L., Atchison, K., Fisher, K.E., Davis, G.E., and Cornelison, D.D.W. (2009). 3D timelapse analysis of muscle satellite cell motility. Stem Cells *27*, 2527–2538. 10.1002/stem.178.
24. Watt, D.J., Morgan, J.E., Clifford, M.A., and Partridge, T.A. (1987). The movement of muscle precursor cells between adjacent regenerating muscles in the mouse. Anat Embryol (Berl) *175*, 527–536. 10.1007/BF00309688.
25. Webster, M.T., Manor, U., Lippincott-Schwartz, J., and Fan, C.-M. (2016). Intravital Imaging Reveals Ghost Fibers as Architectural Units Guiding Myogenic Progenitors during Regeneration. Cell Stem Cell *18*, 243–252. 10.1016/j.stem.2015.11.005.
26. Purslow, P.P. (2020). The Structure and Role of Intramuscular Connective Tissue in Muscle Function. Front Physiol *11*. 10.3389/fphys.2020.00495.
27. Lieber, R.L., and Ward, S.R. (2013). Cellular mechanisms of tissue fibrosis. 4. structural and functional consequences of skeletal muscle fibrosis. Am J Physiol Cell Physiol *305*. 10.1152/ajpcell.00173.2013.
28. Stearns-Reider, K.M., D'Amore, A., Beezhold, K., Rothrauff, B., Cavalli, L., Wagner, W.R., Vorp, D.A., Tsamis, A., Shinde, S., Zhang, C., *et al.* (2017). Aging of the skeletal muscle extracellular matrix drives a stem cell fibrogenic conversion. Aging Cell *16*, 518–528. 10.1111/acel.12578.
29. Hinds, S., Bian, W., Dennis, R.G., and Bursac, N. (2011). The role of extracellular matrix composition in structure and function of bioengineered skeletal muscle. Biomaterials *32*, 3575–3583. 10.1016/j.biomaterials.2011.01.062.
30. Xiaoping, C., and Yong, L. (2009). Role of matrix metalloproteinases in skeletal muscle: Migration, differentiation, regeneration and fibrosis. Cell Adh Migr *3*, 337–341.

31. Denais, C.M., Gilbert, R.M., Isermann, P., McGregor, A.L., te Lindert, M., Weigelin, B., Davidson, P.M., Friedl, P., Wolf, K., and Lammerding, J. (2016). Nuclear envelope rupture and repair during cancer cell migration. Science (1979) *352*, 353–358. 10.1126/science.aad7297.
32. Irianto, J., Xia, Y., Pfeifer, C.R., Athirasala, A., Ji, J., Alvey, C., Tewari, M., Bennett, R.R., Harding, S.M., Liu, A.J., *et al.* (2017). DNA Damage Follows Repair Factor Depletion and Portends Genome Variation in Cancer Cells after Pore Migration. Current Biology *27*, 210–223. 10.1016/j.cub.2016.11.049.
33. Pfeifer, C.R., Xia, Y., Zhu, K., Liu, D., Irianto, J., Morales García, V.M., Santiago Millán, L.M., Niese, B., Harding, S., Deviri, D., *et al.* (2018). Constricted migration increases DNA damage and independently represses cell cycle. Mol Biol Cell *29*, 1948–1962. 10.1091/mbc.E18-02-0079.
34. Earle, A.J., Kirby, T.J., Fedorchak, G.R., Isermann, P., Patel, J., Iruvanti, S., Moore, S.A., Bonne, G., Wallrath, L.L., and Lammerding, J. (2020). Mutant lamins cause nuclear envelope rupture and DNA damage in skeletal muscle cells. Nat Mater *19*, 464–473. 10.1038/s41563-019-0563-5.
35. Mamchaoui, K., Trollet, C., Bigot, A., Negroni, E., Chaouch, S., Wolff, A., Kandalla, P.K., Marie, S., di Santo, J., St Guily, J.L., *et al.* (2011). Immortalized pathological human myoblasts: Towards a universal tool for the study of neuromuscular disorders. Skelet Muscle *1*, 34. 10.1186/2044-5040-1-34.
36. Schindelin, J., Arganda-Carrera, I., Frise, E., Verena, K., Mark, L., Tobias, P., Stephan, P., Curtis, R., Stephan, S., Benjamin, S., *et al.* (2009). Fiji - an Open platform for biological image analysis. Nat Methods *9*. 10.1038/nmeth.2019.Fiji.
37. Mah, L.J., El-Osta, A., and Karagiannis, T.C. (2010). γh2AX: A sensitive molecular marker of DNA damage and repair. Leukemia *24*, 679–686. 10.1038/leu.2010.6.
38. Gupta, A., Hunt, C.R., Chakraborty, S., Pandita, R.K., Yordy, J., Ramnarain, D.B., Horikoshi, N., and Pandita, T.K. (2014). Role of 53BP1 in the Regulation of DNA Double-Strand Break Repair Pathway Choice. Radiat Res *181*, 1–8. 10.1667/RR13572.1.
39. Nakamura, A.J., Rao, V.A., Pommier, Y., and Bonner, W.M. (2010). The complexity of phosphorylated H2AX foci formation and DNA repair assembly at DNA double-strand breaks.
40. Murphy, M.M., Lawson, J.A., Mathew, S.J., Hutcheson, D.A., and Kardon, G. (2011). Satellite cells, connective tissue fibroblasts and their interactions are crucial for muscle regeneration. Development *138*, 3625–3637. 10.1242/dev.064162.
41. Ma, N., Chen, D., Lee, J.H., Kuri, P., Hernandez, E.B., Kocan, J., Mahmood, H., Tichy, E.D., Rompolas, P., and Mourkioti, F. (2022). Piezo1 regulates the regenerative capacity of skeletal muscles via orchestration of stem cell morphological states. Sci Adv *8*, 1–15. 10.1126/sciadv.abn0485.
42. Kuang, S., Gillespie, M.A., and Rudnicki, M.A. (2008). Niche Regulation of Muscle Satellite Cell Self-Renewal and Differentiation. Cell Stem Cell *2*, 22–31. 10.1016/j.stem.2007.12.012.
43. Chapman, M.A., Pichika, R., and Lieber, R.L. (2015). Collagen crosslinking does not dictate stiffness in a transgenic mouse model of skeletal muscle fibrosis. J Biomech *48*, 375–378. 10.1016/j.jbiomech.2014.12.005.

44. Didier, N., Hourdé, C., Amthor, H., Marazzi, G., and Sassoon, D. (2012). Loss of a single allele for Ku80 leads to progenitor dysfunction and accelerated aging in skeletal muscle. EMBO Mol Med *4*, 910–923. 10.1002/emmm.201101075.
45. Puri, P.L., Bhakta, K., Wood, L.D., Costanzo, A., Zhu, J., and Wang, J.Y.J. (2002). A myogenic differentiation checkpoint activated by genotoxic stress. Nat Genet *32*, 585–593. 10.1038/ng1023.
46. Krauss, R.S. (2010). Regulation of promyogenic signal transduction by cell-cell contact and adhesion. Exp Cell Res *316*, 3042–3049. 10.1016/j.yexcr.2010.05.008.
47. Sénéchal, H., Wahrmann, J.P., Delain, D., and Macieira-Coelho, A. (1984). Modulation of differentiation in vitro. II. Influence of cell spreading and surface events on myogenesis. In Vitro *20*, 692–698. 10.1007/BF02618874.
48. Konigsberg, I.R. (1971). Diffusion-mediated control of myoblast fusion. Dev Biol *26*, 133–152. 10.1016/0012-1606(71)90113-8.
49. Kojouharov, H. v., Chen-Charpentier, B.M., Solis, F.J., Biguetti, C., and Brotto, M. (2021). A simple model of immune and muscle cell crosstalk during muscle regeneration. Math Biosci, 108543. 10.1016/j.mbs.2021.108543.
50. Smith, L.R., and Barton, E.R. (2014). Collagen content does not alter the passive mechanical properties of fibrotic skeletal muscle in mdx mice. Am J Physiol Cell Physiol *306*. 10.1152/ajpcell.00383.2013.
51. Juhas, M., Ye, J., and Bursac, N. (2016). Design, evaluation, and application of engineered skeletal muscle. Methods *99*, 81–90. 10.1016/j.ymeth.2015.10.002.
52. Truskey, G.A., Achneck, H.E., Bursac, N., Chan, H.F., Cheng, C.S., Fernandez, C., Hong, S., Jung, Y., Koves, T., Kraus, W.E., *et al.* (2013). Design considerations for an integrated microphysiological muscle tissue for drug and tissue toxicity testing. Stem Cell Res Ther *4*, 1–5. 10.1186/scrt371.
53. Cheng, C.S., Davis, B.N., Madden, L., Bursac, N., and Truskey, G.A. (2014). Physiology and metabolism of tissue-engineered skeletal muscle. Exp Biol Med *239*, 1203–1214. 10.1177/1535370214538589.
54. Khodabukus, A., Prabhu, N., Wang, J., and Bursac, N. (2018). In Vitro Tissue-Engineered Skeletal Muscle Models for Studying Muscle Physiology and Disease. Adv Healthc Mater *7*, 1701498. 10.1002/adhm.201701498.
55. Hu, L.Y., Mileti, C.J., Loomis, T., Brashear, S.E., Ahmad, S., Chellakudam, R.R., Wohlgemuth, R.P., Gionet-Gonzales, M.A., Leach, J.K., and Smith, L.R. (2021). Skeletal muscle progenitors are sensitive to collagen architectural features of fibril size and cross linking. Am J Physiol Cell Physiol *321*, C330–C342. 10.1152/ajpcell.00065.2021.
56. Collet, J.P., Shuman, H., Ledger, R.E., Lee, S., and Weisel, J.W. (2005). The elasticity of an individual fibrin fiber in a clot. Proc Natl Acad Sci U S A *102*, 9133–9137. 10.1073/pnas.0504120102.
57. Yang, L., van der Werf, K.O., Koopman, B.F.J.M., Subramaniam, V., Bennink, M.L., Dijkstra, P.J., and Feijen, J. (2007). Micromechanical bending of single collagen fibrils using atomic force microscopy. J Biomed Mater Res A *82A*, 160–168. 10.1002/jbm.a.31127.
58. Kleinman, H.K., and Martin, G.R. (2005). Matrigel: Basement membrane matrix with biological activity. Semin Cancer Biol *15*, 378–386. 10.1016/j.semcancer.2005.05.004.

59. Hughes, C.S., Postovit, L.M., and Lajoie, G.A. (2010). Matrigel: a complex protein mixture required for optimal growth of cell culture. Proteomics *10*, 1886–1890. 10.1002/pmic.200900758.
60. Bakooshli, M.A., Lippmann, E.S., Mulcahy, B., Iyer, N., Nguyen, C.T., Tung, K., Stewart, B.A., van den Dorpel, H., Fuehrmann, T., Shoichet, M., *et al.* (2019). A 3d culture model of innervated human skeletal muscle enables studies of the adult neuromuscular junction. Elife *8*, 1–29. 10.7554/eLife.44530.
61. Khodabukus, A., Paxton, J.Z., Donnelly, K., Baar, K., Khodabukus, A., Paxton, J.Z., Donnelly, K., and Engineered, K.B. (2007). Engineered Muscle: A Tool for Studying Muscle Physiology and Function muscle: a tool for studying muscle physiology and function.
62. van der Schaft, D.W.J., van Spreeuwel, A.C.C., Boonen, K.J.M., Langelaan, M.L.P., Bouten, C.V.C., and Baaijens, F.P.T. (2013). Engineering skeletal muscle tissues from murine myoblast progenitor cells and application of electrical stimulation. J Vis Exp. 10.3791/4267.
63. Wang, J., Khodabukus, A., Rao, L., Vandusen, K., Abutaleb, N., and Bursac, N. (2019). Engineered skeletal muscles for disease modeling and drug discovery. Biomaterials *221*, 119416. 10.1016/j.biomaterials.2019.119416.
64. Joulia, D., Bernardi, H., Garandel, V., Rabenoelina, F., Vernus, B., & Cabello, G. (2003). Mechanisms involved in the inhibition of myoblast proliferation and differentiation by myostatin. *Experimental Cell Research*, *286*(2), 263–275. 10.1016/S0014-4827(03)00074-0